# UC Irvine
## UC Irvine Previously Published Works

### Title
Modular polymer biosensors by solvent immersion imprint lithography

### Permalink
https://escholarship.org/uc/item/8469f87j

### Journal
Journal of Polymer Science Part B Polymer Physics, 54(1)

### ISSN
0887-6266

### Authors
Moore, Jayven S
Xantheas, Sotiris S
Grate, Jay W
et al.

### Publication Date
2016

### DOI
10.1002/polb.23961

### Copyright Information
This work is made available under the terms of a Creative Commons Attribution License, availalbe at https://creativecommons.org/licenses/by/4.0/

Peer reviewed

eScholarship.org Powered by the California Digital Library
University of California

# Modular Polymer Biosensors by Solvent Immersion Imprint Lithography

**Jayven S. Moore,[1] Sotiris S. Xantheas,[2] Jay W. Grate,[2] Thomas W. Wietsma,[1] Enrico Gratton,[3] Andreas E. Vasdekis[1,4]**

[1]Environmental Molecular Sciences Laboratory, Pacific Northwest National Laboratory, Richland, Washington, 99352
[2]Pacific Northwest National Laboratory, Physical Sciences Division, PO Box 999, Richland, Washington, 99352
[3]Laboratory of Fluorescence Dynamics, Biomedical Engineering Department, University of California, Irvine, California, 92697
[4]Department of Physics, University of Idaho, Moscow, Idaho, 83844
Correspondence to: A. E. Vasdekis (E-mail: andreasv@uidaho.edu)

Received 7 August 2015; accepted 26 October 2015; published online 9 November 2015
**DOI: 10.1002/polb.23961**

**ABSTRACT**: We recently demonstrated Solvent Immersion Imprint Lithography (SIIL), a rapid benchtop microsystem prototyping technique, including polymer functionalization, imprinting and bonding. Here, we focus on the realization of planar polymer sensors using SIIL through simple solvent immersion without imprinting. We describe SIIL's impregnation characteristics, including an inherent mechanism that not only achieves practical doping concentrations, but their unexpected 2-fold enhancement compared to the immersion solution. Subsequently, we developed and characterized optical sensors for detecting molecular $O_2$. To this end, a substantially high dynamic range is reported, including its control through the immersion duration, a manifestation of SIIL's modularity. Overall, SIIL exhibits the potential of improving the operating characteristics of polymer sensors, while significantly accelerating their prototyping, as it requires a few seconds of processing and no need for substrates or dedicated instrumentation. These are critical for $O_2$ sensing as probed by way of example here, as well as any polymer permeable reactant. © 2015 Wiley Periodicals, Inc. J. Polym. Sci., Part B: Polym. Phys. **2016**, *54*, 98–103

**KEYWORDS**: films; gels; imaging; optics; photophysics; sensors

**INTRODUCTION** Polymer sensors have received considerable attention in recent years due to their prototyping simplicity, cost-effectiveness, and compatibility with patient monitoring.[1,2] Since their emergence more than two decades ago, numerous sensing architectures have emerged,[3,4] including novel material systems such as conjugated polymers,[5] nanocolloids,[6] and graphene.[7] Such advances have successfully addressed a wide variety of applications in areas such as security, health, and the environment.[8–10] Generally, such modalities sense the presence or activity of an analyte either electrically or optically, with the latter being substantially more compatible with microscopy and high-throughput applications such as optofluidics[11–14] and microfluidics.[15–17]

Similarly, the optical sensing of oxygen—a widespread electron acceptor in nature—has gained substantial attention.[18] Such sensors are employed in the form of thin films (i.e., planar sensors), either as "patches" on containers, or directly integrated with optical fibers. Application of such planar oxygen sensors typically involved monitoring respiration kinetics in bioreactors, disease diagnostics, fuel tank stability analysis, and food packaging quality control. Additionally, oxygen sensing has been successfully implemented in microfluidics for identifying the impact of oxygen tension on mammalian cells, as well as fundamental metabolic studies in microbial communities that extend even down to the single cell level.[19–21] In both cases of planar and microfluidic integrated oxygen sensors, their prototyping typically involves the spin coating of a polymer solution mixed with an oxygen sensing chromophore,[15–17,22] resulting in a thin sensing film deposited on a substrate; this includes microfluidics designed to image the microfluidic's spatial structure.[16] While the approaches based on spin-coating thin-films accurately control the sensor thickness and doping uniformity, the use of a substrate is far from ideal in applications within liquid or chemically challenging environments that may undermine the film stability, including its delamination. Alternative approaches involve the use of super-critical $CO_2$ mediated impregnation in bulk polymer slabs, thereby eliminating the need of a substrate,[23] as well as sol–gel strategies.[24]

While the previously reported approaches have successfully addressed a plethora of sensing challenges and needs, they usually require dedicated instrumentation and expertise, as well as long and multistep processing, especially in the context of optofluidic sensors. This is particularly pertinent in addressing the inherent photobleaching of phosphorescent

© 2015 Wiley Periodicals, Inc.

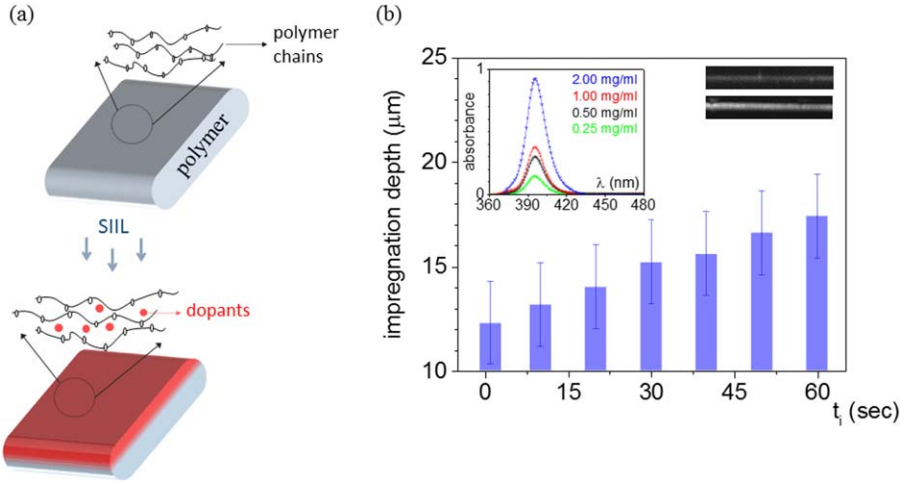


**FIGURE 1** (**a**) A schematic illustration of the SIIL mediated impregnation of the upper surfaces of a polymer slab, thereby giving rise to planar polymer sensors. (**b**) The dependence of the impregnation depth as a function of the solvent immersion time ($t_i$). The insets plot the absorption spectrum of the polymer sensor for different immersion solution concentrations and an immersion time of 30 seconds (**left**) and displays two cross-sectional views of the SIIL sensors using confocal microscopy (**right**) for 10 and 60 seconds immersion durations. [Color figure can be viewed in the online issue, which is available at wileyonlinelibrary.com.]

probes, which necessitates frequent sensing module replacement, thus decreasing cost-effectiveness. To overcome this shortcoming, we have recently demonstrated a substantially faster and simpler alternative process, termed solvent immersion imprint lithography (SIIL).[25] SIIL is beneficial in polymer processing since it employs commonly available solvents for reducing the polymer glass transition temperature. This enables the reduction of polymer interchain interactions and mobility enhancement without the need for dedicated instruments operating under high temperature conditions. Thus, following solvent immersion—a single processing step lasting less than 1 minute—it is possible to prototype a complete polymer microsystem, including imprinting, bonding and three-dimensional (3D) functionalization (or impregnation). Such advantages are pertinent to both optofluidics and microfluidics in life and energy sciences.[26]

Here, we analyze polymer impregnation pertaining to planar sensing modules, one aspect of SIIL that relies only on solvent immersion without imprinting or bonding [Fig. 1(a)]. This simple impregnation step gives rise to uniformly coated polymer slaps at depths controlled simply through the immersion duration. In the following sections, we analyze the mechanism of impregnation during solvent immersion through imaging and spectroscopy. Subsequently, we investigate the optical detection of molecular $O_2$ in SIIL-modified polymer slabs, and by using advanced photophysical characterizations we gain deeper insight into SIIL's modularity for controlling the sensor's dynamic range and sensitivity.

## EXPERIMENTAL

### Sensor Fabrication

To form the sensing slabs, 1.2 mm thick polystyrene (PS) slabs were cut to approximate areas of 1 $cm^2$ (GoodFellow Cambridge Limited, UK). The slabs were then immersed in an acetone solution of the platinum porphyrin compound Pt(II) meso-Tetra(pentafluorophenyl)porphine (PtT975, Frontier Scientific, USA) at specific concentrations. The immersion duration ($t_i$) was controlled with a digital timer. Following immersion, the PS slabs were removed from the solvent and their edge was rapidly brought in contact with a Kimwipe for approximately 2 seconds to remove the excess solvent from their surface. Subsequently, the slabs were placed between two polydimethylsiloxane (PDMS) slabs to dry under low pressure (exerted by a 500 g weight). The evaporation step was found to be as short as 30 seconds for the aforementioned polymer and solvent combination. The PDMS slabs were not structured, and were employed to avoid random morphology modifications of polymer's surface during solvent evaporation. During this process, both the upper and lower surfaces of the polymer slab are impregnated. This had no effect on the sensor characterization, which was performed using a focused excitation and collection from a single surface. We have also achieved a single-surface impregnation simply by coating one of the slab surfaces with epoxy that was readily removed manually due to its poor adhesion from the polymer.

### Impregnation Characterization

To characterize the impregnation mechanism, SIIL-modified polymer slabs were placed on an inverted microscope (Leica DMI6000) coupled with a spinning disk confocal system (Yokogawa CSU10). A 20× objective was used and a z-scan was performed at a 2 μm step size. Additional confocal imaging was performed using the OptiGrid module on a Leica DMI6 inverted microscope, at a step size of 1.2 μm using a similar 20× objective. With both methods, the impregnation was characterized by intensity thresholding. Absorption

spectroscopy was performed using a UV–VIS spectrometer (UV-1700-PharmaSpec, Shimazdu). For this, the same immersed samples were used and the absorption spectra were collected from 190 nm to 800 nm in steps of 1 nm. The imaging and spectroscopic measurements were combined to determine the doping concentration within the polymer matrix.

**Sensor Characterization**

The planar polymer sensors were placed in a sealed chamber, equipped with a silica window for optical access, as well as one inlet and one outlet. The inlet of the chamber was connected with gas impermeable Tygon tubes, comprised of a single long component (~3 m) to enable adequate mixing in line with two additional Tygon tubes through a V connector. The latter two tubes were connected to $N_2$ and $O_2$ gas cylinders through two separate—manually controlled—mass flow controllers (Alicat Scientific MC-55LPM-D/5M, equipped with 8-pin mini-DIN connectors). Prior to characterization, the chamber and sensing films were purged with pure $N_2$ for approximately 40 min. Subsequently, different $O_2$–$N_2$ mixtures were introduced and the sensor was characterized in an inverted optical microscope (Leica DMI6000) coupled with a fluorescence lifetime imaging setup (LI2CAM-P, Lambert Instruments, Netherlands). For oxygen sensing, an LED with an emission spectrum centered at 400 nm modulated at 5 kHz was employed.

**Impregnation with SIIL**

In SIIL processing, a polymer slab is immersed in an organic solvent for a controlled amount of time ($t_i$).[25] Provided that the polymer–solvent system is properly chosen, during the immersion step solvent molecules penetrate the polymer matrix at a rate that is roughly inversely proportional to the cohesive-energy difference between the solvent and the polymer (Hildebrand solubility parameter).[27,28] Two outcomes of solvent penetration are essential to SIIL processing, namely:[25] (1) the gel formation in the upper layers of the polymer slab that enables imprinting/bonding, and (2) the co-transport of solutes dissolved in the solvent that gives rise to polymer impregnation [Fig. 1(a)].

Both the imprinting and impregnation depths can be controlled via the solvent penetration rate or the immersion duration time ($t_i$). We have previously explored in detail the effects of both the type of solvent and the immersion duration time ($t_i$) on imprinting and bonding;[25] here, our specific focus is to elucidate the impregnation process and its impact on the sensing performance of molecular $O_2$.[28] Polystyrene (PS) was chosen as the polymer matrix and acetone as the solvent. The Hildebrand parameters ($\delta$) for acetone and PS are 20.4 $(J/cm^3)^{1/2}$ and 18.7 $(J/cm^3)^{1/2}$, respectively. Such a solubility parameter difference allows for the regulation of the impregnation depth with immersion time [Fig. 1(b) and inset]. In contrast, smaller (larger) differences in the Hildebrand parameters would be characteristic of much faster (practically no) mixing between the solvent and the polymer matrix, leading eventually to complete polymer dissolution. $O_2$ sensing was enabled by the platinum porphyrin compound Pt(II) meso-Tetra(pentafluorophenyl)porphine, dissolved in acetone under variable concentrations ranging from 0.25 up to 2 mg/mL (see "Experimental" section for more details).

**Impregnation Mechanism**

We initially investigated the underlying impregnation process to gain mechanistic insight into the possibilities and limitations in SILL-mediated polymer doping. To this end, PS slabs were immersed for 20 seconds in an acetone–chromophore solution at various concentrations, followed by a brief drying step at room temperature between two pieces of non-structured (PDMS). The impregnation depth ($d$) of the sensing moieties was subsequently analyzed by confocal microscopy to determine its dependence on the immersion duration ($t_i$) (see "Experimental" section). Absorption spectroscopy was subsequently performed on the same polymer slabs [Fig. 1(b), inset] in order to quantify their absorbance ($A$). In this way, the dopant concentration ($c$) in the polymer was determined through the Beer–Lambert law: $c = \frac{A}{2\varepsilon d(t_i)}$, where $\varepsilon = 8.61 \times 10^{-4}$ $M^{-1}$ $cm^{-1}$ is the molar extinction coefficient for the porphyrin complex.[29] The factor of 2 in the denominator stems from the fact that A was measured for both surfaces of the polymer slabs since both were impregnated during SIIL at similar impregnation depths (data not shown). The results, shown in Figure 2(a), indicate that the concentration of dopant in the polymer matrix increases linearly with the dopant concentration in the immersion solution. This was confirmed by the high Pearson's coefficient of the linear fitting ($r = 0.99$), with a slope of approximately 2. This slope value indicates essentially that the embedded chromophore concentration in the polymer matrix is two-fold enhanced compared with that of the immersion solution.

To further investigate this practical enhancement mechanism, we varied the immersion time ($t_i$) for all different solution concentrations (0.25–2 mg/mL). By taking into consideration the associated variation of the impregnation depth [Fig. 1(b)], we confirmed the linear correlation between the polymer doping versus the solution concentration for all immersion durations. The slope of such linear fits (i.e., the enhancement factor) is approximately 2 for all immersion durations, with the exception of immersion durations $t_i$ less than 10 seconds. This gives rise to the "dose-response" curve illustrated in the inset of Figure 2(a). Such a complex dependence of the doping enhancement on $t_i$ is indicative of the underlying polymer–solvent interactions and the resulting diffusion-mediated kinetics of the solvent penetration in the polymer.[27,28] During solvent immersion of the polymer slab [Fig. 2(b)], the solvent diffuses within the polymer (to typical depths in excess of 10 $\mu$m depending on the immersion time) simultaneously carrying the chromophores as a result of the strong interactions between the dopant molecules and acetone (via $\pi$—OH, C—F···O and H···O bonds). Furthermore, a second solvent transport process is involved in the SIIL planar sensor development. This occurs during the drying step, when the solvent escapes the polymer slab

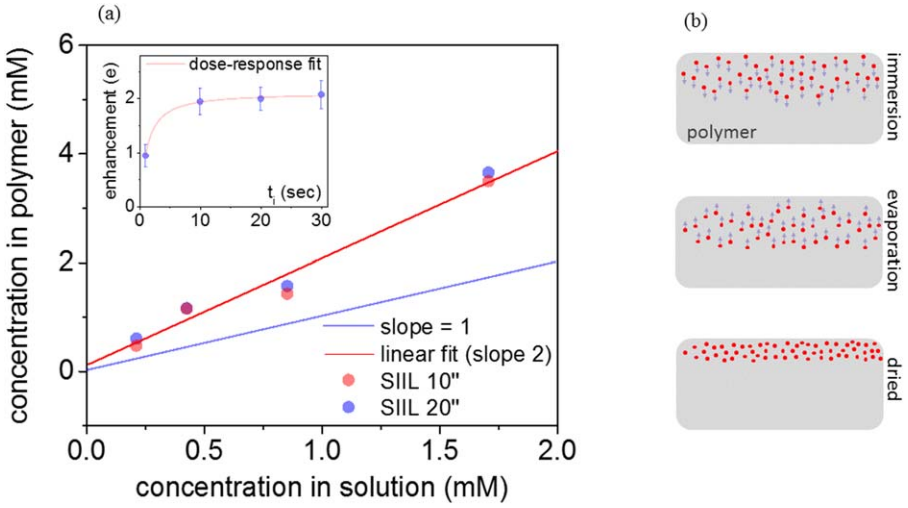


**FIGURE 2** (**a**) The chromophore doping concentration within the polymer matrix as a function of the solution concentration; the experimental data are denoted by the *blue circles*, the *red line* indicates a linear fit and the *blue line* the 1:1 relationship between the chromophore concentration in the polymer and in the solution. The inset plots the enhancement factor of the polymer doping concentration as a function of the immersion time; the *blue line* denotes the dose–response curve. (**b**) A schematic illustration of the immersion and evaporation mediated transport of the chromophore solution (*red circles*) in the polymer slab (*gray*), as well as the resulting enhanced doping concentration in the polymer matrix. [Color figure can be viewed in the online issue, which is available at wileyonlinelibrary.com.]

through evaporation [Fig. 2(b)]. This in essence reverses the solvent transportation with respect to solvent immersion. During solvent evaporation, however, the chromophores are also carried toward the surface of the polymer slab through the strong solvent–chromophore interactions, overcoming the weaker chromophore–polymer interactions (via $\pi$–$\pi$ bonds between the chromophore's and polystyrene's benzene rings). This 2-way transport mechanism is the likely origin of the observed enhanced chromophore concentration at layers closer to the polymer surface in comparison to their concentration in solution (Fig. 2).

### Oxygen Response

To analyze the response to gaseous $O_2$, polymer sensors were fabricated as previously described by simple solvent immersion and drying in-between two flat PDMS stamps. The SIIL sensors were subsequently introduced in a sealed chamber, including a silica window for optical access. Therein, $N_2$ and $O_2$ gases were introduced and mixed at different ratios and the sensor response was analyzed by using a FLIM imaging set-up capable of capturing both intensity and lifetime images. A typical intensity and lifetime Stern–Volmer quenching plot is illustrated in Figure 3(a) for a SIIL sensor obtained by immersing PS in an acetone solution of the sensing dye (1 mg/mL concentration). The graph plots the $I_0/I$ and $\tau_0/\tau$ namely the intensity ($I$) and lifetime ($\tau$) sensor response under different $O_2$ concentrations with respect to the values under zero $O_2$ concentration ($I_0$, $\tau_0$). The immersion duration was 30 seconds, resulting in an impregnation depth of approximately $15 \pm 2$ $\mu$m [cf. Fig. 1(b)]. Figure 3(a) illustrates that below a 20% $O_2$ concentration, the lifetime and intensity quenching plots essentially overlap. However, a substantial deviation is observed above a concentration of 20% $O_2$, indicating the involvement of both dynamic and static quenching mechanisms upon the interaction of the sensing dye with molecular oxygen.[30] This is better visualized in Figure 3(b) that shows the sensor's lifetime and intensity responses in alternating exposures to pure $O_2$ and $N_2$. It is worth noting that the implication of both quenching mechanisms does not limit the sensor's dynamic range. On the contrary, static quenching enhances the intensity-based detection range—especially above a 20% $O_2$ concentration [Fig. 3(a)]—without hindering the repeatability, as also evidenced by time-lapse FLIM experiments in Figure 3(b).

Additionally, the Stern–Volmer plot exhibits a downward non-linearity for both the intensity and lifetime curves at high $O_2$ concentrations (>80%). This is a typical response from chromophores embedded in a solid matrix, manifesting the heterogeneous matrix microenvironment. The latter gives rise to combined responses from complexes that exhibit variable accessibility to oxygen.[31,32] Such microheterogeneity is further suggested by the phasor plot of the FLIM images, illustrated in Figure 3(c) for three $O_2$ concentrations.[33] All three measurements deviate from the phasor plot's universal circle, indicating the involvement of multiexponential decays. Such micro-heterogeneity is anticipated during SIIL processing, similar to almost all other methods of prototyping polymer sensors (e.g., spin-coating).

### SIIL Modularity

In addition to its simplicity, SIIL exhibits enhanced modularity in sensor design through the control of the immersion

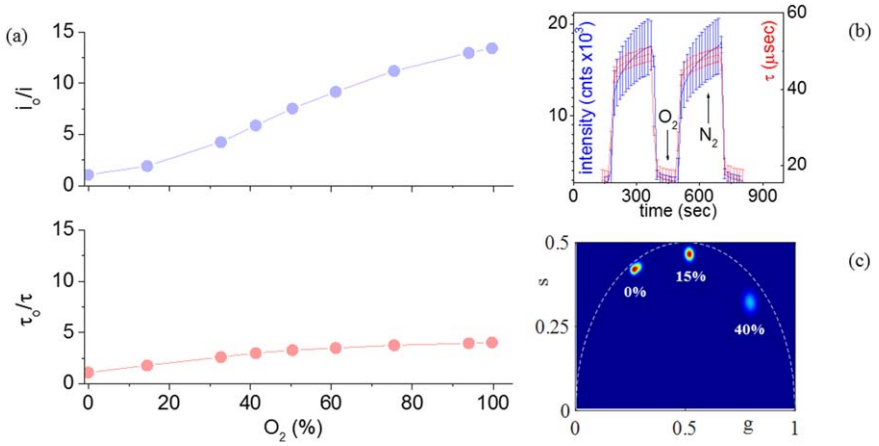


**FIGURE 3** (**a**) Typical Stern–Volmer quenching plots for both the intensity (**upper**) and lifetime (**lower**) for a polymer film impregnated with the oxygen sensing dye by immersion in an acetone dye solution at a concentration of 1 mg/mL for 30 seconds. (**b**) Time-lapse FLIM imaging of both the intensity and lifetime, where the gas flown over the sensor was manually controlled from 100% $N_2$ to 100% $O_2$; error bars denote the standard deviation of the intensity or lifetime over the FLIM image. (**c**) A phasor histogram plot of the same film for three oxygen concentrations, viz. 0%, 15%, and 40%; the x- and y- axes denote the $g_{i,j}(\omega)=m_{i,j}\cdot\cos(\varphi_{i,j})$ and $s_{i,j}(\omega)=m_{i,j}\cdot\sin(\varphi_{i,j})$ components, where [i,j] are the pixel indices, and $m$ and $\varphi$ are the modulation and the phase of the emission with respect to the excitation and $\omega=2\pi\nu$, where $\nu$ was the 5 kHz modulation frequency employed in the FLIM analysis. [Color figure can be viewed in the online issue, which is available at wileyonlinelibrary.com.]

solution's chromophore concentration, as well as the immersion duration time. Regarding the former, the intensity quenching plot for variable doping densities at a 30 seconds immersion time is illustrated in Figure 4(a). Up to approximately 40% $O_2$, the quenching curves overlap to a high degree indicating that all chromophores in the matrix respond in a similar fashion within this range. Above this level, however, a minor divergence between each concentration emerges, with the highest dynamic range demonstrated by the lowest immersion solution concentration.

On the contrary, by varying the immersion duration time a considerable modulation of the sensor response is enabled. This is plotted in Figure 4(b) for a PS sensor realized by immersion at a concentration solution of 1 mg/mL. The different immersion durations enable a substantially divergent response even above the 10% $O_2$ concentration border. The origin of this behavior emanates from the different thicknesses

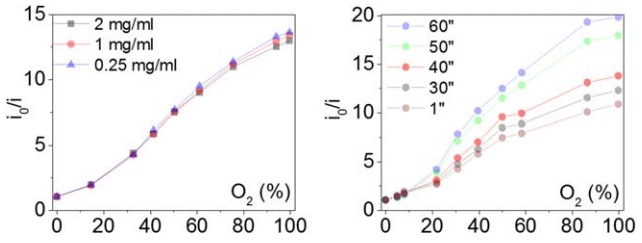


**FIGURE 4** Intensity calibration plots for planar polymer sensors by simple solution immersion without imprinting. Solutions of different chromophore concentrations were employed but at the same immersion time ($t_i=30$ seconds) (**a**), as well as different immersion times at 1 mg/mL chromophore concentration in solution (**b**). [Color figure can be viewed in the online issue, which is available at wileyonlinelibrary.com.]

of the sensing layer due to the different immersion duration times, and thus the different diffusional barriers to molecular $O_2$ they represent [Fig. 1(b)]. $O_2$ transport within the polymer is not instantaneous but rather undergoes Fickian diffusion with a constant of $4\times10^{-8}$ $cm^2/s$.[25] Thus, by simply controlling the immersion duration time, the sensing dynamic range can be increased more than two-fold, in essence enabling one of the highest dynamic ranges ever reported.[15,22]

## CONCLUSION

In conclusion, we reported the realization of planar polymer sensors using SIIL. The impregnation mechanism was first analyzed using microscopy and spectroscopy, unmasking a two-fold enhanced doping concentration in the polymer matrix with respect to the corresponding one in the immersion solution. Such enhancement enables practical doping levels even under immersion in dilute solutions. We demonstrated such sensors, exhibiting a high dynamic range that could be further controlled through the immersion duration time, thus revealing SIIL's modularity. Overall, SIIL significantly improves planar polymer sensor prototyping by enabling extremely short processing duration times, while at the same time eliminating the need for substrates or dedicated instrumentation. These are critical not only in sensing—including scintillator applications—but also in chemical synthesis within polymer reactors, as well as in complete optofluidic microsystems as we have previously reported.[25]

## ACKNOWLEDGMENTS

AEV gratefully acknowledges funding from the Pacific Northwest National Laboratory (Linus Pauling Fellowship – LDRD

project ID: PN12005/2406), as well as from the INBRE Program, NIH Grant (National Institute of General Medicine Sciences – Project ID: P20 GM103408). Part of the research was performed using EMSL, a national scientific user facility sponsored by the Department of Energy's Office of Biological and Environmental Research and located at Pacific Northwest National Laboratory (proposal ID: 48924). SSX was supported by the US Department of Energy, Office of Science, Office of Basic Energy Sciences, Division of Chemical Sciences, Geosciences and Biosciences. Pacific Northwest National Laboratory (PNNL) is a multiprogram national laboratory operated for DOE by Battelle. EG acknowledges funding from NIH P41-GM103540 and JWG partial support by the Laboratory Directed Research and Development Program at Pacific Northwest National Laboratory (PNNL) in a technology supporting program.

## REFERENCES AND NOTES

**1** B. Adhikari, S. Majumdar, *Prog. Polym. Sci.* **2004**, *29*, 699–766.

**2** A. K. Bansal, S. Hou, O. Kulyk, E. M. Bowman, I. D. W. Samuel, *Adv. Mater.* **2014**, doi:10.1002/adma.201403560.

**3** C. Preininger, I. Klimant, O. S. Wolfbeis, *Anal. Chem.* **1994**, *66*, 1841–1846.

**4** O. S. Wolfbels, *Anal. Chem.* **2008**, *80*, 4269–4283.

**5** D. T. McQuade, A. E. Pullen, T. M. Swager, *Chem. Rev.* **2000**, *100*, 2537–2574.

**6** M. Lorenzon, S. Christodoulou, G. Vaccaro, J. Pedrini, F. Meinardi, I. Moreels, S. Brovelli, *Nat. Commun.* **2015**, *6*, doi: 10.1038/ncomms7434.

**7** G. S. Kulkarni, K. Reddy, Z. Zhon, X. Fan, *Nat. Commun.* **2014**, *5*, doi:10.1038/ncomms5376.

**8** S. J. Toal, W. C. Trogler, *J. Mater. Chem.* **2006**, *16*, 2871–2883.

**9** R. Moos, N. Izu, F. Rettig, S. Reiß, W. Shin, I. Matsubara, *Sensors* **2011**, *11*, 3439–3465.

**10** J. I. Peterson, G. G. Vurek, *Science* **1984**, *224*, 123–127.

**11** D. Psaltis, S. R. Quake, C. Yang, *Nature* **2006**, *442*, 381–386.

**12** X. Fan, I. M. White, *Nat. Photon.* **2011**, *5*, 591–597.

**13** J. G. Cuennet, A. E. Vasdekis, L. De Sio, D. Psaltis, *Nat. Photon.* **2011**, *5*, 234–238.

**14** D. Erickson, D. Sinton, D. Psaltis, *Nat. Photon.* **2011**, *5*, 583–590.

**15** A. P. Vollmer, R. F. Probstein, R. Gilbert, T. Thorsen, *Lab Chip* **2005**, *5*, 1059–1066.

**16** J. W. Grate, R. T. Kelly, J. Suter, N. C. Anheier, *Lab Chip* **2012**, *12*, 4796–4801.

**17** L. Gitlin, C. Hoera, R. J. Meier, S. Nagl, D. Belder, *Lab Chip* **2013**, *13*, 4134–4141.

**18** R. Ramamoorthy, P. K. Dutta, S. A. Akbar, *J. Mater. Sci.* **2003**, *38*, 4271–4282.

**19** L.-L. Zhu, L.-Y. Wu, D. T. Yew, M. Fan, *Mol. Neurobiol.* **2005**, *31*, 231–242.

**20** T. W. Molter, S. C. McQuaide, M. T. Suchorolski, T. J. Strovas, L. W. Burgess, D. R. Meldrum, M. E. Lidstrom, *Sensors Actuat. B-Chem.* **2009**, *135*, 678–686.

**21** A. E. Vasdekis, G. Stephanopoulos, *Metab. Eng.* **2015**, *27*, 115–135.

**22** V. Nock, R. J. Blaikie, T. David, *Lab Chip* **2008**, *8*, 1300–1307.

**23** S. P. Nalawade, F. Picchioni, L. Janssen, *Prog. Polym. Sci.* **2006**, *31*, 19–43.

**24** C.-S. Chu, C.-Y. Chuang, *Sens. Actuators B-Chem.* **2015**, *209*, 94–99.

**25** A. E. Vasdekis, M. J. Wilkins, J. W. Grate, R. T. Kelly, A. E. Konopka, S. S. Xantheas, T.-M. Chang, *Lab Chip* **2014**, *14*, 2072–2080.

**26** K. S. Elvira, R. C. R Wootton, N. M. Reis, M. R. Mackley, A. J. deMello, *ACS Sustain. Chem. Eng.* **2013**, *1*, 209–213.

**27** F. Asmussen, K. Ueberreiter, *J. Polym. Sci.* **1962**, *57*, 199.

**28** B. A. Miller-Chou, J. L. Koenig, *Progr. Polym. Sci.* **2003**, *28*, 1223–1270.

**29** D.-H. Won, M. Toganoh, H. Unob, H. Furuta, *Dalton Trans.* **2009**, *2009*, 6151–6158.

**30** P. Hartmann, M. J. P. Leiner, M. E. Lippitsch, *Sens. Actuators B-Chem.* **1995**, *29*, 251–257.

**31** J. R. Bacon, J. N. Demas, *Anal. Chem.* **1987**, *59*, 2780–2785.

**32** W. Y. Xu, R. C. McDonough III, B. Langsdorf, J. N. Demas, B. A. DeGraff, *Anal. Chem.* **1994**, *66*, 4133–4141.

**33** C. Stringari, A. Cinquin, O. Cinquin, M. A. Digman, P. J. Donovan, E. Gratton, *Proc. Natl. Acad. Sci. USA* **2011**, *108*, 13582–13587.